# Scene Graph Generation from Hierarchical Relationship Reasoning

# Bowen Jiang, Camillo J. Taylor University of Pennsylvania

{bwjiang, cjtaylor}@seas.upenn.edu

# **Abstract**

This paper presents a novel approach for inferring relationships between objects in visual scenes. It explicitly exploits an informative hierarchical structure that can be imposed to divide the object and relationship categories into disjoint super-categories. Specifically, our proposed method incorporates a Bayes prediction head, enabling joint predictions of the super-category as the type of relationship between the two objects, along with the detailed relationship within that super-category. This design reduces the impact of class imbalance problems. Furthermore, we also modify the supervised contrastive learning to adapt our hierarchical classification scheme. Experimental evaluations on the Visual Genome and OpenImage V6 datasets demonstrate that this factorized approach allows a relatively simple model to achieve competitive performance, particularly in predicate classification and zero-shot tasks.

#### 1. Introduction

This work considers the Scene Graph Generation problem, initially proposed by Johnson et al. [10]. In this framing, the objective is to deduce the objects present in an image and their interconnected relationships. Unlike standard object detection [26, 28, 19, 1] or segmentation [7, 20, 29, 2] algorithms, which focus on identifying individual object instances, scene graph generation algorithms represent the entire scene as a directed graph. In scene graphs, each object instance is a node, and the relationships between a pair of objects are represented as directed edges. Triplets of a subject, an object, and a relationship, such as <person, wear, skirt> and <bunny, on, lawn>, are often referred to as motifs [39] and form essential components of a scene graph. The rich knowledge encoded in scene graphs finds applications in various downstream tasks like image retrieval [22] and visual scene understanding [24, 10].

Zeller et al. [39] observe that the categories associated with the subject and object instances in an image are strongly predictive of the relationship between them. For instance, a "woman" and a "shirt" are likely to have a "wears"

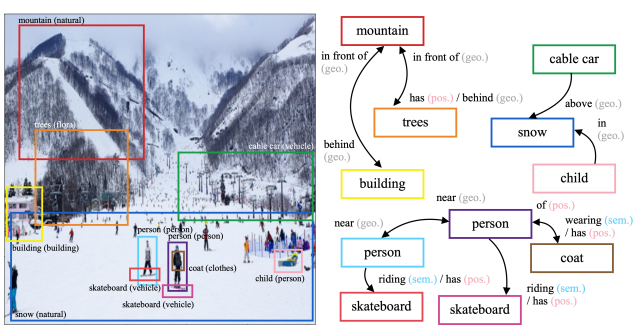


Figure 1. Example scene graph. Each bounding box represents an object instance labeled by its category. Relationships between objects are represented by arrows, and colored labels indicate relationship super-categories: geometric, possessive, and semantic.

relationship. Building upon this insight, the authors go further and show that when the objects are divided into super-categories such as "Animal", "Vehicle", and "Furniture", and the relationships between objects are similarly divided into three super-categories "Geometric", "Possessive", and "Semantic", the object categories and supercategories become strongly predictive of the relationship super-categories. For example, the relationship between a person and an article of clothing is likely to be possessive in nature. Based on this observation, the authors argue in favor of approaches that condition relationship predictions on these subject and object categories.

In this work, we take inspiration from the aforementioned idea and introduce a novel approach to scene graph construction that leverages an informative hierarchical structure. To the best of our knowledge, we are the first authors that directly exploit and fully utilize the informative hierarchical structures that divide the object and relationship categories into disjoint super-categories. We show that a relatively straightforward network that exploits this hierarchical structure can outperform state-of-the-art methods.

Specifically, our proposed network considers each subject-object pair in an image and generates the following outputs: a scalar value indicating relationship existence, the probabilities of relationship super-categories, and the conditional probabilities of specific relationship classes within

each super-category. Besides, we modify the supervised contrastive learning algorithm [12] to adapt our hierarchical classification scheme. The resulting network effectively captures a structure from the Bayes' rule where the probabilities associated with the super-categories serve to steer the attention of the network to the most profitable lines of interpretation.

We dub our model *HierMotif* as it exploits hierarchical knowledge in motifs. Through comprehensive numerical experiments, we demonstrate the effectiveness of our method, particularly in predicate classification tasks and zero-shot learning, by employing hierarchical relationship reasoning. Our contributions can be summarized as follows:

To summarize our contributions:

- 1. We show that a simple scene graph generation model can achieve superior performance by leveraging object and relationship hierarchies.
- We propose a novel classification scheme inspired by Bayes' rule, which jointly predicts relationship supercategory probabilities and conditional probabilities of relationships within each super-category.
- 3. We modify the supervised contrastive learning algorithm to adapt the hierarchical classification scheme, further enhancing the network's performance.
- 4. We perform experiments with extensive ablation studies and zero-shot learning to validate the effectiveness of our proposed algorithms.

The structure of this manuscript is as follows: Section 2 discusses related work, Section 3 presents the details of our model, including the Bayes prediction head, and finally, Section 4 provides the experimental results.

## 2. Related Work

Our work considers the scene graph generation problems proposed in [10] and [21]. Many authors have approached the problem from the graphical neural networks perspective [30, 35, 37, 18, 3, 11]. IMP [35] uses iterative message passing to update node and edge features in a bipartite graph. Graph-RCNN [37] prunes unlikely relationships and uses an attentional graph convolution network [13] to integrate global contexts and update nodes and edges.

Recurrent neural networks [39, 35, 4, 6] have also played important roles in scene graph generation as a means for integrating global context information across the image. For example, node and edge features in [35] are represented by two GRUs [4], which take incoming messages and produce new hidden states. Neural Motifs [39] investigates the repeated motif structures in scene graphs and captures global contexts with bidirectional LSTMs [9].

In their work on Neural Motifs, Zellers et al. [39] analyze scene graphs in the Visual Genome [15] dataset and divide the 150 most frequently encountered object categories

into 17 super-categories and the 50 most frequently encountered relationship categories into 3 relationship supercategories: *geometric*, *possessive*, and *semantic*, as illustrated in Table 1. However, their proposed algorithm does not explicitly exploit the super-categories they identify. Our work follows their super-category classifications and fully utilizes this hierarchy information. We discover that the median relative frequency of a relationship label is only 0.17%, but when we divide them into super-categories, this median frequency increases to 0.79% (geometric), 1.4% (possessive), and 2.3% (semantic), respectively.

Super-categories	Categories	Num
Geometric	above, behind, between, near,	15
Possessive	belonging to, has, of, part of,	11
Semantic	wears, carrying, eating, riding,	. 24

Table 1. The relationship hierarchy in [39] and some examples under each super-category. Our work follows the same definitions.

In recent years, BGT-Net [6] utilizes a bidirectional GRU for instance-level communications, an object transformer encoder to predict instance categories, and another edge transformer encoder to generate edge information for every instance. HC-Net [27] works on scene graph generation with hierarchical contexts, rather than the hierarchies of objects and relationships we exploit. GPS-Net [18] focuses on recovering the direction of the relationship edges and understanding the relative priority of the nodes in the graph within a novel message-passing scheme. RTN [14] presents a relation transformer network with a node-to-node encoder and a node-to-edge decoder. RelTR [5] also employs a Detection Transformer (DETR) [1] backbone, but it proposes a complicated triplet decoder network with three sub-modules and takes subject and object queries as input tokens. [36] establishes a unified conditional random field to model the distribution of objects and relationships jointly. Besides, [31] offers an energy-based framework instead of cross-entropy loss to incorporate the structure of the scene graph.

# 3. Method

#### 3.1. Notation

A scene graph  $G=\{V,E\}$  is a graphical representation of a given image. The set of vertices V consists of n object instances, including their bounding boxes  $\{b_i \mid b_i \in \mathbb{R}^4\}$ , the object categories  $\{c_i \mid c_i \in \mathbb{N}\}$  and their super-categories. **Bold** symbols denote vectors instead of scalars, except  $\mathbf{p}$  stands for the probability operator. The set of edges, E, consists of relationships  $\{r_{ij} \mid r_{ij} \in \mathbb{N}\}$  between each pair of instances and their relationship supercategory. We assume each pair of objects have one relationship  $r_{ij}$  annotated. Both i and j ranges from 1 to n, so the total number of possible  $r_{ij}$  is  $n^2$ . For every possible edge,

we predict a connectivity score  $\{e_{ij} \mid e_{ij} \in [0,1]\}$ , which models whether a pair of object instances are connected.

## 3.2. Scene Graph Construction

Our scene understanding system in Figure 2 constructs a scene graph by considering each pair of object instances in turn and predicting whether or not they are related and, if so, what kind of relationship pertains.

Object detection backbone Our scene graph generation system adopts the widely-used two-stage model design [35, 37, 39, 18, 6] where we first utilize a pre-trained object detection backbone to predict object bounding boxes and labels, and subsequently predict relationships between the detected objects. To this end, we leverage the powerful Detection Transformer (DETR) [1] object detection module as the front end of our system. DETR has a ResNet-101 feature extraction backbone [8], followed by a transformer encoder [1, 34] designed to effectively contextualize global image features from ResNet into each element of the encoder output using self-attention mechanism. The transformer encoder output preserves its spatial dimensions and serves as the contextualized image features  $I \in \mathbb{R}^{h \times s \times t}$ , where h refers to the number of hidden dimensions, and sand t denote its two spatial dimensions.

On the output side, a transformer decoder, equipped with a feed-forward head [1, 34] predicts the final set of object predictions, encompassing object classes and their corresponding bounding boxes. The decoder employs crossattention to utilize the contextualized image features as keys and values in relation to the object queries.

Additionally, for precise depth estimation, we employ the MiDaS [25] single-image depth estimation network, which provides estimated depth maps  $\boldsymbol{D}$  for input images. Depth maps are then concatenated to the contextualized image features along the hidden dimension. The integration of depth information enhances the ability of our system to capture depth-related relationships. The final image features  $\boldsymbol{I}' = \operatorname{concat}\{\boldsymbol{I}, \boldsymbol{D}\} \in \mathbb{R}^{(h+1)\times s\times t}$  serve as the input of the subsequent networks for relationship reasoning.

**Direction-aware multiplicative masking** After extracting image features I', our next step considers each pair of object instances to reason about their relationships. Global contexts have already been contextualized in the backbone, so we refer to the rest of the system as the local predictor.

For every pair of objects, we construct a combined feature tensor by converting their bounding boxes into two binary masks  $M_i, M_j \in \mathbb{R}^{s \times t}$ , where bounding boxes are either the gound-truth boxes provided or predicted by the DETR backbone. These masks are then element-wise multiplied with the image features I', resulting in two different feature tensors  $I'_i, I'_j \in \mathbb{R}^{(h+1) \times s \times t}$ : one for an instance

in the pair. These tensors are concatenated to a tensor in  $\mathbb{R}^{2(h+1)\times s\times t}$  and passed on to the subsequent stage.

Notably, the order of these two object tensors is important. For example, motifs  $\langle bike \rangle$  has, wheel $\rangle$  and  $\langle wheel \rangle$  of, bike $\rangle$  depend on which instance is considered as the subject and which one as the object. Therefore, we perform two separate passes through our relationship network, depicted in Figure 2. One pass considers  $I'_i$  as the subject and  $I'_j$  as the object and concatenates them as  $I'_{ij}$ , while the other pass swaps their roles and concatenates them as  $I'_{ji}$ . Instead of using a union mask, such concatenations preserve the direction information of two object instances, and also handle well the cases where two masks have large overlaps.

Unlike [39, 6, 38] that crop objects by their RoI regions and resize them to a uniform size as their object features, our strategy maintains the instance size information, the spatial locations of each instance in the whole image, and the relative locations between each subject-object pair. Ablation studies show significant performance improvements by effectively retaining spatial and directional information.

Subsequently, the subject-object feature tensors  $I_{ij}'$  are fed into a network comprising two convolutional layers, and the output will be flattened as a 1-d hidden vector. Four one-hot vectors, encoding the categories and super-categories associated with the subject and the object, are concatenated to the hidden vector. Same as bounding boxes, they are either the ground truth or predicted by the DETR backbone. Two additional linear layers reduce this concatenated vector, yielding a final 512-dimensional hidden vector denoted as  $X_{ij}$ . This hidden vector encapsulates information derived from both the feature tensors and the associated categories and super-categories, benefitting the subsequent Bayes prediction head.

**Bayes prediction head** The Bayes prediction head is structured to produce multiple interpretable quantities, drawing inspiration from the Bayes' rule. Firstly, it generates a scalar connectivity score  $e_{ij} \in [0,1]$ , indicating the likelihood of a relationship existing between object instances i and j.

Additionally, the head outputs three scalar values  $r_{ij}^{\rm sc} \in \mathbb{R}^3 = [\mathbf{p}(\text{geo}), \ \mathbf{p}(\text{pos}), \ \mathbf{p}(\text{sem})]$ , representing the probabilities that, if a relationship exists, it belongs to the geometric, possessive, or semantic super-categories, respectively.

Finally, the network produces three vectors that are interpreted as conditional probability distributions:  $\boldsymbol{r}_{ij}^{\mathrm{geo}} = \mathbf{p}(\boldsymbol{\tilde{r}}_{ij}^{\mathrm{geo}}|\mathrm{geo}) \in \mathbb{R}^{15}$  denotes the probability of labeling the relationship as each of the 15 categories under the geometric relationship super-category, conditioned on the relationship belonging to that super-category. Similarly,  $\boldsymbol{r}_{ij}^{\mathrm{pos}} = \mathbf{p}(\boldsymbol{\tilde{r}}_{ij}^{\mathrm{pos}}|\mathrm{pos}) \in \mathbb{R}^{11}$  and  $\boldsymbol{r}_{ij}^{\mathrm{sem}} = \mathbf{p}(\boldsymbol{\tilde{r}}_{ij}^{\mathrm{sem}}|\mathrm{sem}) \in \mathbb{R}^{24}$  denote the conditional probabilities associated with the possessive and semantic super-category, respectively.

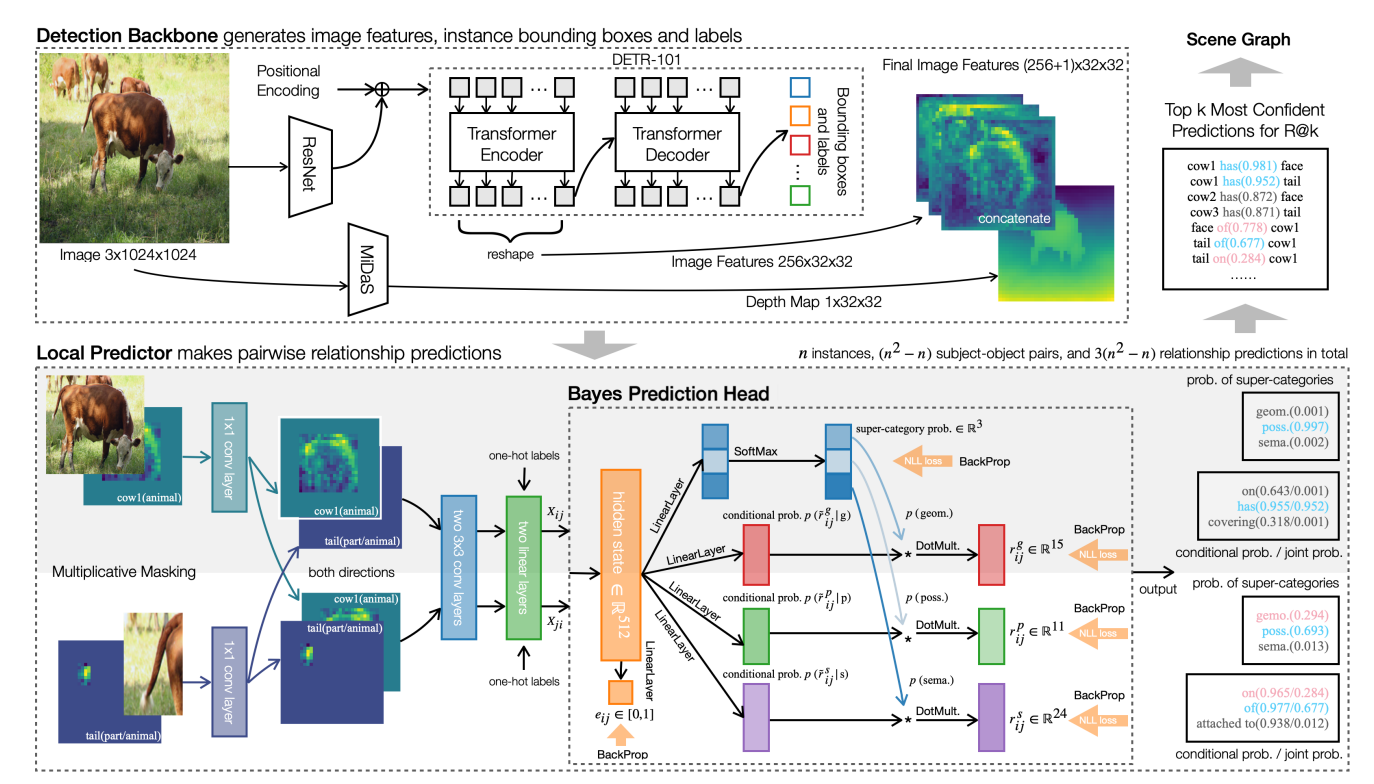


Figure 2. Illustration of our scene graph construction scheme. The DETR detection backbone generates image features, instance bounding boxes, and labels. The local predictor focuses on predicting pairwise relationships. For a pair of object proposals i and j, we conduct two *separate* passes through our relationship network, one with i as the subject and j as the object, and another with j as the subject and i as the object. In each pass, the Bayes prediction head predicts the super-category distribution and the conditional probabilities under each super-category, generating three hypotheses for the relationship, one for each super-category. Pink predicates are true positives, blue predicates are reasonably true predictions not yet annotated in the dataset, and gray predicates are false positives. All predicates are ranked by their confidence for the final recall scores.

Figure 2 and Equations 1-5 show how these quantities are combined to produce final classification results trainable via back-propagation. The output score vectors associated with each relationship category,  $r_{ij}^{\text{geo}} \in \mathbb{R}^{15}$ ,  $r_{ij}^{\text{pos}} \in \mathbb{R}^{11}$ , and  $r_{ij}^{\text{sem}} \in \mathbb{R}^{24}$ , are computed by multiplying the conditional probability vectors with their associated supercategory probabilities. Assuming \* is the scalar product,

$$e_{ij} = \text{Sigmoid}\left\{\boldsymbol{X}_{ij}^{\top} \boldsymbol{W}^{\text{conn}}\right\}$$
 (1)

$$\boldsymbol{r}_{ij}^{\mathrm{sc}} = \operatorname{SoftMax} \left\{ \boldsymbol{X}_{ij}^{\mathsf{T}} \boldsymbol{W}^{\mathrm{sc}} \right\}$$
 (2)

$$r_{ij}^{\text{geo}} = \operatorname{Softmax} \left\{ \boldsymbol{X}_{ij}^{\top} \boldsymbol{W}^{\text{geo}} * \mathbf{p}(\text{geo}) \right\}$$
 (3)

$$r_{ij}^{\text{pos}} = \text{Softmax}\left\{\boldsymbol{X}_{ij}^{\top} \boldsymbol{W}^{\text{pos}} * \mathbf{p}(\text{pos})\right\}$$
 (4)

$$r_{ij}^{\text{sem}} = \text{Softmax} \left\{ \boldsymbol{X}_{ij}^{\top} \boldsymbol{W}^{\text{sem}} * \mathbf{p}(\text{sem}) \right\},$$
 (5)

where all  $\boldsymbol{W}$  in these equations are the learnable parameter tensors of linear layers. Equation 1-5 can be summarized as

$$[e_{ij}, \boldsymbol{r}_{ij}^{\text{sc}}, \boldsymbol{r}_{ij}^{\text{geo}}, \boldsymbol{r}_{ij}^{\text{pos}}, \boldsymbol{r}_{ij}^{\text{sem}}] = \text{BayesHead} \{\boldsymbol{X}_{ij}\}.$$
 (6)

with the loss function

$$\mathcal{L}_{\text{conn}} = \text{BCE Loss } \{e_{ij}, \underline{e_{ij}}\}$$
 (7)

$$\mathcal{L}_{\text{rel}} = \sum_{c \in \{\text{sc,geo,pos,sem}\}} \text{NLL Loss } \{\boldsymbol{r}_{ij}^c, \underline{r}_{ij}^c\}, \qquad (8)$$

where underline denotes corresponding ground truths. Softmax in 1-5 combined with negative log-likelihood loss in 8 is equivalently the cross-entropy loss.

The module finally generates three relationship predictions, one for each super-category, by considering the maximum entry in each of the vectors  $r_{ij}^{\rm g}$ ,  $r_{ij}^{\rm p}$ , and  $r_{ij}^{\rm s}$ . The associated maximum entries are multiplied by the connectivity score,  $e_{ij}$ , to produce a final score for each relationship hypothesis. These maximum entries, multiplied by the connectivity score,  $e_{ij}$ , result in a final score for each relationship hypothesis. These scores are then used to rank order the relationship hypotheses from all subject-object pairs, providing insights into the most probable relationships in the whole scene graph.

Notably, this design leverages the super-category probabilities to guide the network's attention toward the appropri-

ate conditional output heads, enhancing the interpretability and performance of the system. The use of separate linear layers does not exacerbate scalability issues, as it involves a nearly identical number of model parameters as a single larger linear layer in  $\mathbb{R}^{50}$ .

**Supervised Contrastive Loss** Supervised contrastive loss [12] is designed to encourage the network to bring similar samples closer and push dissimilar samples apart in the learned feature space. In the case of scene graph generation, for each data sample in a batch, the contrastive loss minimizes the distance between positive pairs (hidden states  $X_{ij}$  that share the same relationship) and maximizes the distance between negative pairs (hidden states  $X_{ij}$  that have different relationships).

However, in a hierarchical setting with three disjoint super-categories, the traditional supervised contrastive loss might not be fully appropriate. For a given subject-object pair, only one of the actual relationships under one supercategory may be annotated, but unlabeled relationships under a different super-category may still be valid, and the contrastive loss should not penalize them. Therefore, it is essential to modify the supervised contrastive loss in [12] to take into account the hierarchical structure and only contrast hidden embeddings within each disjoint parent class.

The modified supervised contrastive loss function for each sample  $X_{ij}$  in a batch is as follows.

$$\mathcal{L}_{\text{contrast}} = \frac{-1}{|P(ij)|} \sum_{p \in P(ij)} \log \frac{\exp\left(\boldsymbol{X}_{ij} \cdot \boldsymbol{X}_p / \tau\right)}{\sum_{n \in N(ij)} \exp\left(\boldsymbol{X}_{ij} \cdot \boldsymbol{X}_n / \tau\right)}$$
(9)

Here, the symbol  $\cdot$  denotes the matrix product,  $\tau$  is the temperature, the set P(ij) represents the indices of all positive samples in the batch with the same relation as the current one, and N(ij) represents the set of indices of all samples with different relations but still *within* the same relation super-category with the current one. It ignores all the others under different super-categories.

The final loss function for training is  $\mathcal{L}_{rel} + \lambda_{conn} * \mathcal{L}_{conn} + \lambda_{contrast} * \mathcal{L}_{contrast}$ , where all  $\lambda$  are tuning parameters set to 1 in all of our experiments.

#### 4. Experimental Results

#### 4.1. Dataset

**Visual Genome** We perform comprehensive experiments on the Visual Genome dataset [15], following the same preprocessing procedure used in [35] to clean up object annotations. The dataset comprises the most frequent 150 object categories and 50 relationship predicates. These categories are organized into 17 object super-categories and 3 relationship super-categories following [39]. With approximately

75.7k training images and 32.4k testing images, each image, on average, contains 11.5 object instances and 6.2 relationships.

**OpenImage V6** We follow the same data pre-processing provided by [17] to obtain a subset of the OpenImage V6 dataset [16] with relationship annotations. It has 601 object categories, 30 relationship categories, about 53.9k training images, and around 3.2k testing images.

#### 4.2. Evaluation metrics

**Visual Genome** We employ the Recall@k (R@k) [21] and mean Recall@k (mR@k) [33] evaluation metrics that are widely used for this dataset. R@k measures the fraction of ground-truth predicates that appear in the top k most confident predictions per image. The mR@k metric provides an average recall score across all 50 relationship categories. A ground truth predicate is considered a match when the predicted relationship is correct, the subject and object labels match, and the bounding boxes associated with the subject and object have an Intersection over Union (IOU) of at least 0.5 with the ground-truth boxes.

Our hierarchical relationship scheme generates three predictions per direction under three *disjoint* supercategories for each edge. Consequently, each directed edge produces three individual candidates that can be ranked in the top k most confident predictions, as depicted in Figure 2.

We also provide evaluation metrics  $R@k^*$  and  $mR@k^*$ , offering more insight into the accuracy of the prediction head associated with the relationship super-categories. For these metrics, if any one of the three super-category output heads correctly predicts the relationship, we score it as a match. Unlike NG-R@k [23, 39] that uses a "no graph constraint" and loosely defines a match based on any of the 50 predicates with non-zero scores, our  $R@k^*$  is more stringent, as it maintains exclusivity among predicates within the same super-category. In other words, each edge has a maximum of three chances to be marked as correct.

Zero-shot recall (zsR@k) [32] estimates the model's ability to generalize its performance to unseen data. It calculates the R@k score for the triplets that only appear in the testing dataset, but not in the training dataset.

**OpenImage V6** On this challenge we consider the standard evaluation metrics: Recall@50 (R@50), weighted mean average prevision of relationships (wmAP<sub>rel</sub>), weighted mean average prevision of phrases (wmAP<sub>phr</sub>), and the final score =  $0.2 \times R@50+0.4 \times \text{wmAP}_{rel} + 0.4 \times \text{wmAP}_{phr}$  [40]. wmAP<sub>rel</sub> counts a match if both the subject and object bounding boxes have IOU  $\geq 0.5$  with their ground-truths, and the <subject, relationship, and object>labels match with the target. Same for wmAP<sub>phr</sub> except it considers the union bounding box of the subject and object.

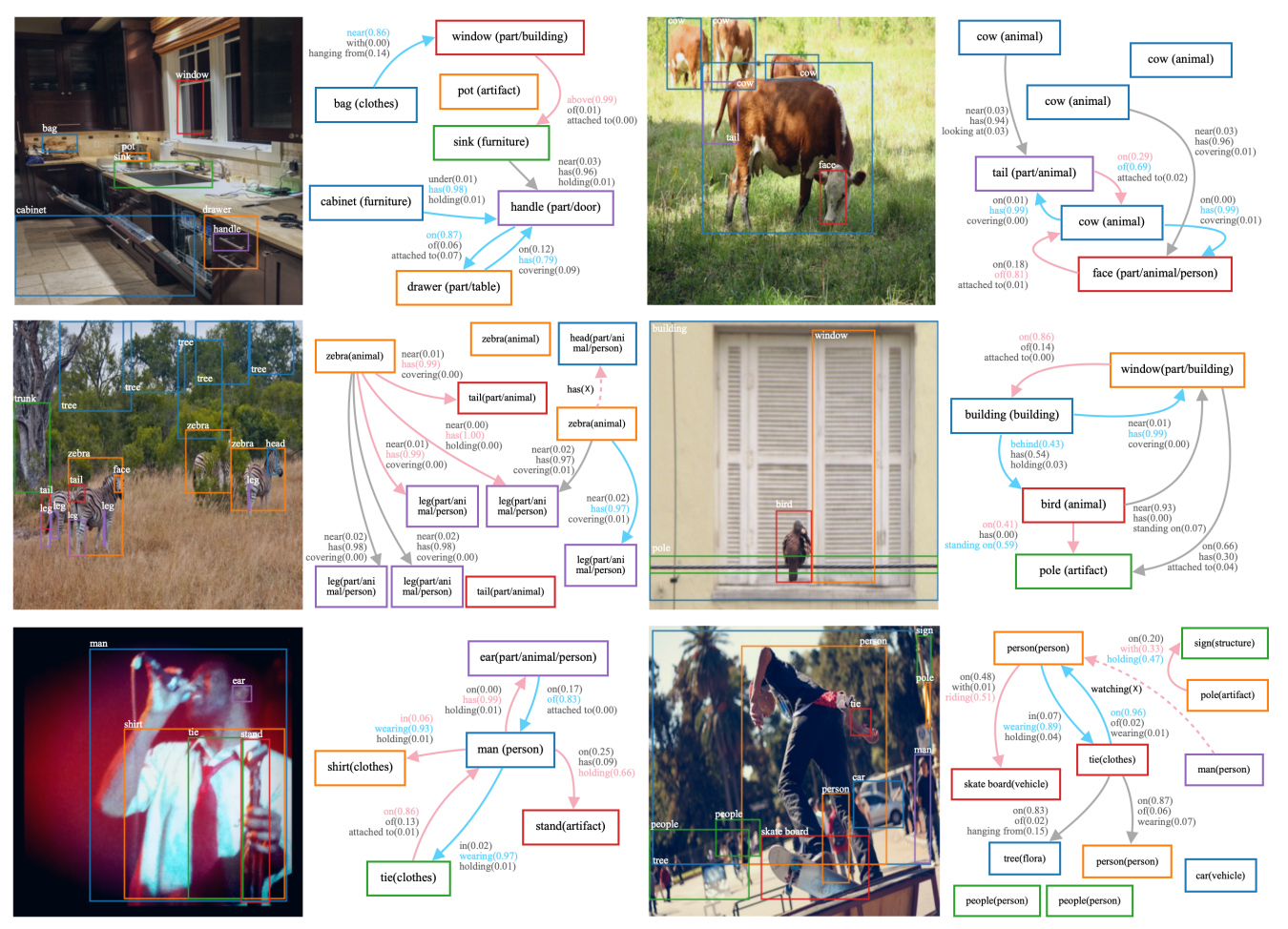


Figure 3. Illustrations of scene graphs produced by our model for the PredCLS task. All samples come from the Visual Genome test dataset. Each edge is annotated with 3 possible labels, one for each relationship super-category, along with the confidence scores of super-categories. We include edges that contain predicates among the top 5 most confident predictions and other true positive predictions within the top 20. We sketch four types of arrows: (1) solid pink arrow: true positive predicates. (2) dotted pink arrow: false negative predicates. (3) solid blue arrow: reasonably true positives predicates not yet annotated in the dataset. (4) solid gray arrow: false positive predicates.

## 4.3. Evaluation modes

Predicate classification (PredCLS) focuses solely on relationship prediction, separating it from other procedures. Given a set of ground-truth object instance labels and bounding boxes, the model predicts relationships. Scene graph classification (SGCLS) predicts subject, object, and relationship categories using ground-truth bounding boxes. In our experiment, the DETR backbone outputs bounding boxes and labels simultaneously without a separate region proposal network [28], so we match each ground-truth box with a predicted box having the largest IOU.

Scene graph detection (SGDET) involves predicting instance bounding boxes, object labels, and relationships, requiring adaptations for handling noisy bounding boxes and labels. We incorporate per-class non-maximum suppression (NMS), dismiss non-overlapping pairs [39], duplicate pre-

dicted bounding boxes with top two most confident object labels, and account for ambiguous object categories.

## 4.4. Training details

All models are trained on four NVIDIA V100 GPUs. The average inference time per image is 0.16 seconds when predicting all predicates in parallel. To generate object bounding boxes and labels, we leverage the pretrained DETR detection backbone from [17], while keeping its model parameters frozen when training subsequent models.

Despite the necessity of evaluating every possible pair of object instances to make inferences on an image, the efficiency of training the model remains intact due to the sparsity of target relationship annotations used for backpropagation. Our model, with an approximate size of 1055 MB, was effectively trained using a batch size of 16 for 3 epochs on the Visual Genome dataset or 1 epoch on the OpenImage

	PredCLS		SGCLS			SGDET			
Methods	R@20	R@50	R@100	R@20	R@50	R@100	R@20	R@50	R@100
IMP [35]	-	44.8	53.1	-	21.7	24.4	-	3.4	4.2
GraphRCNN [37]	-	54.2	59.1	-	29.6	31.6	-	11.4	13.7
NeuralMotifs [39]	58.5	65.2	67.1	32.9	35.8	36.5	21.4	27.2	30.3
Motif+EB [31]	58.4	65.2	67.3	35.7	39.1	40.0	24.3	31.7	36.3
HC-Net [27]	59.6	66.4	68.8	34.2	36.6	37.3	22.6	28.0	31.2
GPS-Net [18]	60.7	66.9	68.8	36.1	39.2	40.1	22.6	28.4	31.7
BGT-Net [6]	60.9	67.3	68.9	38.0	40.9	43.2	23.1	28.6	32.2
RelTR [5]	63.1	64.2	-	29.0	36.6	-	21.2	27.5	-
HierMotifs* (ours)	69.1	77.9	80.0	35.8	39.7	40.5	27.2	32.3	33.5
HierMotifs (ours)	63.3	74.7	78.4	32.3	37.7	39.5	24.4	30.4	33.0
	mR@20	mR@50	mR@100	mR@20	mR@50	mR@100	mR@20	mR@50	mR@100
NeuralMotifs [39]	11.7	14.8	16.1	6.7	8.3	8.8	4.9	6.8	7.9
Motif+EBM [31]	14.2	18.0	19.5	8.2	10.2	11.0	5.7	7.7	9.3
GPS-Net [18]	17.4	21.3	22.8	10.0	11.8	12.6	6.9	8.7	9.8
BGT-Net [6]	16.8	20.6	23.0	10.4	12.8	13.6	5.7	7.8	9.3
RelTR [5]	20.0	21.2	-	7.7	11.4	-	6.8	10.8	-
HierMotifs* (ours)	21.5	25.5	26.8	12.6	14.9	15.9	8.1	10.2	11.2
HierMotifs (ours)	16.0	21.6	24.3	8.5	11.5	13.7	5.1	8.4	10.5

Table 2. Comparison of test results on Visual Genome over 4 random seeds. We omit the error bars because all standard deviations are below one percent. The top two results are shown in **bold**, and "-" denotes unreported results. We utilize R@k and mR@k, except \* indicates  $R@k^*$  and  $mR@k^*$ . The last row of each sub-table shows that our method, HierMotif, outperforms most state-of-the-art methods on the PredCLS task by a large margin and has good performance on SGCLS and SGDET. Each penultimate row shows that our super-category prediction head is even more effective at identifying the correct relationship.

V6 dataset. To optimize the training process, we utilize the SGD optimizer with a learning rate of 0.0001, along with a step scheduler. All codes are implemented in PyTorch.

#### 4.5. Results

Visual Genome Table 2 presents a comparison of our results on Visual Genome with other state-of-the-art methods. Our model, HierMotif, achieves significant performance gains over previous approaches in the PredCLS task, surpassing them by 6% and 9% on R@50 and R@100, respectively. The penultimate row shows our  $R@k^*$  and  $mR@k^*$  scores, highlighting the strong performance of the super-category prediction subsystems. These results demonstrate that the individual Bayes prediction heads have effectively learned to predict relationships within their respective super-categories.

Methods	zsR@20/50		zs-mR@20/50		
NeuralMotifs [39]	1.4	3.6	-	-	
Motif+EB [31]	2.1	4.9	-	-	
VC-TDE+EB [31]	9.6	15.1	-	-	
Ours	11.1	18.2	3.2	7.0	
Ours no rel-hier	9.9	15.5	2.8	4.2	

Table 3. Zero-shot recall for PredCLS on Visual Genome over 4 random seeds. In the last row, "no rel-hier" means no relation hierarchy, i.e., an ablation model without the Bayes prediction head.

Figure 3 exhibits a collection of generated scene graphs for the PredCLS task on Visual Genome, showcasing the model's ability to produce a diverse range of high-confidence predicates to describe visual scenes. It is in-

triguing to note that the model's true capabilities might be underestimated by existing evaluation metrics due to limited ground-truth annotations in the dataset. Numerous reasonable predictions, aligned with human intuition yet unannotated in the datasets, are marked by blue arrows in the figure. We strongly believe that creating an extensive set of predicates is beneficial for practical scene understanding.

Table 3 illustrates the compelling zero-shot performance on Visual Genome. Notably, the bottom row shows an ablation study where we omit the Bayes prediction head, and we can observe a clear inferiority in performance, emphasizing the crucial role of this component in the model's success.

**OpenImage V6** Table 4 demonstrates the experimental results on the OpenImage V6 dataset, showcasing an outstanding recall scores. Our model makes predictions on all subject-object pairs and outputs the top 20 most confident predictions for each image, so it's precision score  $\mathrm{wmAP}_{\mathrm{rel}}$  still has room to improve, but  $\mathrm{wmAP}_{\mathrm{phr}}$  and the final score already demonstrate competitive performance.

Methods	R@50	$wmAP_{rel}$	$\text{wmAP}_{phr}$	score
SGTR [1]	59.9	37.0	38.7	42.3
RelDN [40]	72.8	29.9	30.4	38.7
GPS-Net [18]	74.7	32.8	33.9	41.6
Ours	85.4	33.1	44.9	48.3

Table 4. Comparison of test results on OpenImage V6 over 4 random seeds. Top one results are shown in **bold**. Our model achieves prominent results in all evaluation metric compared wit other methods.

Ablation studies Table 5 shows ablation studies on the Visual Genome dataset to validate our key design decisions. Firstly, we investigate how our system would fare if we simply used a flat relationship categorization, instead of the hierarchical organization into three relationship supercategories using the Bayes prediction head. The performance is shown on the second row of the table, which is much worse than the hierarchical baseline. It suggests that our hierarchical organization enhances performance, allowing our purposely simplistic relationship prediction scheme to perform competitively against other methods.

On the third row, we examine the results when we disregard the super-categories associated with object instances. This analysis reveals that object super-categories are beneficial, though not as critical as relationship super-categories. Nevertheless, the decrease in mR@k indicates that object super-category information helps share knowledge across related classes, thereby improving performance, particularly when object categories are infrequently encountered.

Subsequently, the fourth row indicates that the image depth maps also help with the predictions. The fifth row evaluates the performance of a variant that replaces the direction-aware multiplicative masking scheme used to extract subject and object features with union bounding boxes. The inferiority emphasizes the importance of retaining awareness of the spatial and direction information between two object instances, enabling the model to better distinguish between two object instances being evaluated.

The next two rows show that the model performs better with our modified contrastive learning. The original supervised contrastive learning [12] also enhances the results, but it is slightly inferior to the modified version.

The final rows of the table present results obtained by varying various hyperparameters related to the SGDET task. This includes experimenting with the number of times we duplicate each predicted bounding box, as well as the non-maximal suppression. The observed differences are minor, but we actually favor small differences because it means the model is more robust to these hyper-parameters.

#### 5. Limitations

The algorithm follows a standard two-stage pipeline, therefore, its performance is upper-bounded by the object detection backbone in scene graph classification and detection tasks. The accuracy of predicted bounding boxes and labels during the object detection step directly impacts the quality of predicted relationships.

The problem of long-tailed distributions remains challenging in scene graph generation. Our model would still bias towards the most frequently appearing predicates, leading to suboptimal performance on less common relationships. We are investigating algorithms that specifically tackle the long tail, and our Bayesian prediction head can

In PredCLS	R@20	R@50	mR@20	mR@50
Final	63.6	74.7	15.3	21.6
No rel-hierarchy	56.3	64.7	11.3	13.5
No ins-hierarchy	62.5	73.3	14.2	19.7
No depth map	62.9	73.7	13.6	19.2
Union bbox	56.3	69.2	12.7	18.6
No SupCon	60.5	73.2	14.8	21.5
SupCon in [12]	62.3	74.0	15.1	21.6
In SGDET	R@20	R@50	mR@20	mR@50
Final	21.8	28.0	4.6	7.4
No duplicate	21.3	27.8	4.0	6.2
NMS 0.7	21.2	27.7	4.5	6.8
NMS 0.3	21.6	27.4	4.5	7.2

Table 5. We show ablation studies on Visual Genome over 4 random seeds in PredCLS. Results prove that object and relation hierarchies, direction-aware multiplicative masking strategy, and supervised contrastive learning remarkably improve relationship predictions. In this table, "No rel-hierarchy" refers to using a flat relationship classification instead of the Bayes prediction head. "No ins-hierarchy" means omitting instance supercategories. "No depth map" means omitting depth maps. "Union bbox" means using union bounding boxes of subject-object pairs, not the direction-aware scheme. "No SupCon" means omitting supervised contrastive loss. "Supcon in [12]" means using the original contrastive loss proposed in [12]. In SGDET, we tune some hyper-parameters. The final model duplicates predicted boxes twice with top 2 most confident object labels and 0.5 per-class NMS, and it is robust to these hyper-parameters.

be seamlessly integrated with such solutions.

# 6. Concluding remarks

We present a straightforward yet powerful scene graph generation algorithm that effectively exploits the object and relationship hierarchies. The resulting system adopts a Bayesian prediction head, enabling simultaneous prediction of both the super-categories and specific relationships within each super-category. This representation effectively factorizes the final probability distribution over the relation categories. As far as we know, we are the first authors to fully exploit these hierarchical structures in the dataset for relationship reasoning in scene graph generations.

Experimental results demonstrate the superiority of our hierarchical organization over a flat classification baseline. Remarkably, it performs competitively with state-of-the-art algorithms, despite its simplicity, especially in predicate classification and zero-shot learning tasks. We posit that the hierarchical structure facilitates more efficient sharing of information among related labels within each super-category.

The proposed hierarchical approach could be applied to other classification tasks, such as attribute learning. It can also be incorporated into existing or future scene graph algorithms, offering an opportunity to improve their results with limited additional complexity, and we are exploring these possibilities in future work.

### References

- [1] Nicolas Carion, Francisco Massa, Gabriel Synnaeve, Nicolas Usunier, Alexander Kirillov, and Sergey Zagoruyko. End-to-end object detection with transformers. In *European conference on computer vision*, pages 213–229. Springer, 2020. 1, 2, 3, 7
- [2] Liang-Chieh Chen, George Papandreou, Iasonas Kokkinos, Kevin Murphy, and Alan L Yuille. Deeplab: Semantic image segmentation with deep convolutional nets, atrous convolution, and fully connected crfs. *IEEE transactions on pattern* analysis and machine intelligence, 40(4):834–848, 2017.
- [3] Tianshui Chen, Weihao Yu, Riquan Chen, and Liang Lin. Knowledge-embedded routing network for scene graph generation. In *Proceedings of the IEEE/CVF Conference on Computer Vision and Pattern Recognition*, pages 6163–6171, 2019.
- [4] Kyunghyun Cho, Bart Van Merriënboer, Dzmitry Bahdanau, and Yoshua Bengio. On the properties of neural machine translation: Encoder-decoder approaches. arXiv preprint arXiv:1409.1259, 2014. 2
- [5] Yuren Cong, Michael Ying Yang, and Bodo Rosenhahn. Reltr: Relation transformer for scene graph generation. *arXiv preprint arXiv:2201.11460*, 2022. 2, 7
- [6] Naina Dhingra, Florian Ritter, and Andreas Kunz. Bgt-net: Bidirectional gru transformer network for scene graph generation. In *Proceedings of the IEEE/CVF Conference on Computer Vision and Pattern Recognition*, pages 2150–2159, 2021. 2, 3, 7
- [7] Kaiming He, Georgia Gkioxari, Piotr Dollár, and Ross Girshick. Mask r-cnn. In *Proceedings of the IEEE international conference on computer vision*, pages 2961–2969, 2017. 1
- [8] Kaiming He, Xiangyu Zhang, Shaoqing Ren, and Jian Sun. Deep residual learning for image recognition. In *Proceedings of the IEEE conference on computer vision and pattern recognition*, pages 770–778, 2016. 3
- [9] Sepp Hochreiter and Jürgen Schmidhuber. Long short-term memory. *Neural computation*, 9(8):1735–1780, 1997.
- [10] Justin Johnson, Ranjay Krishna, Michael Stark, Li-Jia Li, David Shamma, Michael Bernstein, and Li Fei-Fei. Image retrieval using scene graphs. In *Proceedings of the IEEE conference on computer vision and pattern recognition*, pages 3668–3678, 2015. 1, 2
- [11] Mahmoud Khademi and Oliver Schulte. Deep generative probabilistic graph neural networks for scene graph generation. In *Proceedings of the AAAI Conference on Artificial Intelligence*, volume 34, pages 11237–11245, 2020. 2
- [12] Prannay Khosla, Piotr Teterwak, Chen Wang, Aaron Sarna, Yonglong Tian, Phillip Isola, Aaron Maschinot, Ce Liu, and Dilip Krishnan. Supervised contrastive learning. *Advances in neural information processing systems*, 33:18661–18673, 2020. 2, 5, 8
- [13] Thomas N Kipf and Max Welling. Semi-supervised classification with graph convolutional networks. arXiv preprint arXiv:1609.02907, 2016. 2
- [14] Rajat Koner, Suprosanna Shit, and Volker Tresp. Relation transformer network. arXiv preprint arXiv:2004.06193, 2020.

- [15] Ranjay Krishna, Yuke Zhu, Oliver Groth, Justin Johnson, Kenji Hata, Joshua Kravitz, Stephanie Chen, Yannis Kalantidis, Li-Jia Li, David A Shamma, et al. Visual genome: Connecting language and vision using crowdsourced dense image annotations. *International journal of computer vision*, 123(1):32–73, 2017. 2, 5
- [16] Alina Kuznetsova, Hassan Rom, Neil Alldrin, Jasper Uijlings, Ivan Krasin, Jordi Pont-Tuset, Shahab Kamali, Stefan Popov, Matteo Malloci, Alexander Kolesnikov, et al. The open images dataset v4: Unified image classification, object detection, and visual relationship detection at scale. *Interna*tional Journal of Computer Vision, 128(7):1956–1981, 2020.
- [17] Rongjie Li, Songyang Zhang, and Xuming He. Sgtr: End-to-end scene graph generation with transformer. In *Proceedings of the IEEE/CVF Conference on Computer Vision and Pattern Recognition*, pages 19486–19496, 2022. 5, 6
- [18] Xin Lin, Changxing Ding, Jinquan Zeng, and Dacheng Tao. Gps-net: Graph property sensing network for scene graph generation. In *Proceedings of the IEEE/CVF Conference* on Computer Vision and Pattern Recognition, pages 3746– 3753, 2020. 2, 3, 7
- [19] Wei Liu, Dragomir Anguelov, Dumitru Erhan, Christian Szegedy, Scott Reed, Cheng-Yang Fu, and Alexander C Berg. Ssd: Single shot multibox detector. In *European con*ference on computer vision, pages 21–37. Springer, 2016. 1
- [20] Jonathan Long, Evan Shelhamer, and Trevor Darrell. Fully convolutional networks for semantic segmentation. In Proceedings of the IEEE conference on computer vision and pattern recognition, pages 3431–3440, 2015. 1
- [21] Cewu Lu, Ranjay Krishna, Michael Bernstein, and Li Fei-Fei. Visual relationship detection with language priors. In European conference on computer vision, pages 852–869. Springer, 2016. 2, 5
- [22] Roozbeh Mottaghi, Xianjie Chen, Xiaobai Liu, Nam-Gyu Cho, Seong-Whan Lee, Sanja Fidler, Raquel Urtasun, and Alan Yuille. The role of context for object detection and semantic segmentation in the wild. In *Proceedings of the IEEE conference on computer vision and pattern recognition*, pages 891–898, 2014. 1
- [23] Alejandro Newell and Jia Deng. Pixels to graphs by associative embedding. Advances in neural information processing systems, 30, 2017. 5
- [24] Aude Oliva and Antonio Torralba. The role of context in object recognition. *Trends in cognitive sciences*, 11(12):520– 527, 2007.
- [25] René Ranftl, Katrin Lasinger, David Hafner, Konrad Schindler, and Vladlen Koltun. Towards robust monocular depth estimation: Mixing datasets for zero-shot cross-dataset transfer. *IEEE transactions on pattern analysis and machine* intelligence, 2020. 3
- [26] Joseph Redmon, Santosh Divvala, Ross Girshick, and Ali Farhadi. You only look once: Unified, real-time object detection. In *Proceedings of the IEEE conference on computer* vision and pattern recognition, pages 779–788, 2016. 1
- [27] Guanghui Ren, Lejian Ren, Yue Liao, Si Liu, Bo Li, Jizhong Han, and Shuicheng Yan. Scene graph generation with hi-

- erarchical context. *IEEE Transactions on Neural Networks and Learning Systems*, 32(2):909–915, 2020. 2, 7
- [28] Shaoqing Ren, Kaiming He, Ross Girshick, and Jian Sun. Faster r-cnn: Towards real-time object detection with region proposal networks. *Advances in neural information processing systems*, 28, 2015. 1, 6
- [29] Olaf Ronneberger, Philipp Fischer, and Thomas Brox. Unet: Convolutional networks for biomedical image segmentation. In *International Conference on Medical image computing and computer-assisted intervention*, pages 234–241. Springer, 2015. 1
- [30] Franco Scarselli, Marco Gori, Ah Chung Tsoi, Markus Hagenbuchner, and Gabriele Monfardini. The graph neural network model. *IEEE transactions on neural networks*, 20(1):61–80, 2008.
- [31] Mohammed Suhail, Abhay Mittal, Behjat Siddiquie, Chris Broaddus, Jayan Eledath, Gerard Medioni, and Leonid Sigal. Energy-based learning for scene graph generation. In Proceedings of the IEEE/CVF conference on computer vision and pattern recognition, pages 13936–13945, 2021. 2,
- [32] Kaihua Tang, Yulei Niu, Jianqiang Huang, Jiaxin Shi, and Hanwang Zhang. Unbiased scene graph generation from biased training. In Proceedings of the IEEE/CVF conference on computer vision and pattern recognition, pages 3716– 3725, 2020. 5
- [33] Kaihua Tang, Hanwang Zhang, Baoyuan Wu, Wenhan Luo, and Wei Liu. Learning to compose dynamic tree structures for visual contexts. In *Proceedings of the IEEE/CVF con*ference on computer vision and pattern recognition, pages 6619–6628, 2019. 5
- [34] Ashish Vaswani, Noam Shazeer, Niki Parmar, Jakob Uszkoreit, Llion Jones, Aidan N Gomez, Łukasz Kaiser, and Illia Polosukhin. Attention is all you need. *Advances in neural information processing systems*, 30, 2017. 3
- [35] Danfei Xu, Yuke Zhu, Christopher B Choy, and Li Fei-Fei. Scene graph generation by iterative message passing. In *Proceedings of the IEEE conference on computer vision and pattern recognition*, pages 5410–5419, 2017. 2, 3, 5, 7
- [36] Minghao Xu, Meng Qu, Bingbing Ni, and Jian Tang. Joint modeling of visual objects and relations for scene graph generation. *Advances in Neural Information Processing Systems*, 34:7689–7702, 2021. 2
- [37] Jianwei Yang, Jiasen Lu, Stefan Lee, Dhruv Batra, and Devi Parikh. Graph r-cnn for scene graph generation. In *Proceedings of the European conference on computer vision (ECCV)*, pages 670–685, 2018. 2, 3, 7
- [38] Jiaxuan You, Rex Ying, Xiang Ren, William Hamilton, and Jure Leskovec. Graphrnn: Generating realistic graphs with deep auto-regressive models. In *International conference on machine learning*, pages 5708–5717. PMLR, 2018. 3
- [39] Rowan Zellers, Mark Yatskar, Sam Thomson, and Yejin Choi. Neural motifs: Scene graph parsing with global context. In *Proceedings of the IEEE conference on computer vision and pattern recognition*, pages 5831–5840, 2018. 1, 2, 3, 5, 6, 7
- [40] Ji Zhang, Kevin J Shih, Ahmed Elgammal, Andrew Tao, and Bryan Catanzaro. Graphical contrastive losses for scene

graph parsing. In *Proceedings of the IEEE/CVF Conference on Computer Vision and Pattern Recognition*, pages 11535–11543, 2019. 5, 7